Journal of Nuclear Materials 415 (2011) S360–S364

Contents lists available at ScienceDirect

Journal of Nuclear Materials

journal homepage: www.elsevier.com/locate/jnucmat

Dependence of divertor heat flux widths on heating power, flux expansion, and plasma current in the NSTX

T.K. Gray [a,b,*], R. Maingi [b], V.A. Soukhanovskii [c], J.E. Surany [d], J.-W. Ahn [b], A.G. McLean [b]

[a] Oak Ridge Institute for Science and Education (ORISE), Oak Ridge, TN, USA
[b] Oak Ridge National Laboratory, Oak Ridge, TN, USA
[c] Lawrence Livermore National Laboratory, Livermore, CA, USA
[d] Princeton University, Princeton, NJ, USA

ARTICLE INFO

Article history:
Available online 28 January 2011

ABSTRACT

We report the dependence of the lower divertor surface heat flux profiles, measured from infrared thermography and mapped magnetically to the mid-plane on loss power into the scrape-off layer (P_{LOSS}), plasma current (I_p), and magnetic flux expansion (f_{exp}), as well as initial results with lithium wall conditioning in NSTX. Here we extend previous studies [R. Maingi et al., J. Nucl. Mater. 363–365 (2007) 196–200] to higher triangularity ~0.7 and higher $I_p \leqslant 1.2$ MA. First we note that the mid-plane heat flux width mapped to the mid-plane, λ_q^{mid}, is largely independent of P_{LOSS} for $P_{LOSS} \geqslant 4$ MW. λ_q^{mid} is also found to be relatively independent of f_{exp}; peak heat flux is strongly reduced as f_{exp} is increased, as expected. Finally, λ_q^{mid} is shown to strongly contract with increasing I_p such that $\lambda_q^{mid} \propto I_p^{-1.6}$ with a peak divertor heat flux of $q_{div,\ peak} \sim 15$ MW/m^2 when $I_p = 1.2$ MA and $P_{LOSS} \sim 6$ MW. These relationships are then used to predict the divertor heat flux for the planned NSTX-Upgrade, with heating power between 10 and 15 MW, $B_t = 1.0$ T and $I_p = 2.0$ MA for 5 s.

1. Introduction

Spherical tori (ST) face the prospect of high heat flux onto the plasma facing components (PFC), owing to their compact nature and design as high power density systems. The divertor heat flux profile and its characteristic scale length, λ_q^{div} are determined by the balance of parallel and perpendicular thermal transport in the scrape-off layer (SOL), along with volumetric losses along the open field lines [1]. Near term research in this area at the National Spherical Torus Experiment (NSTX) [2] has been motivated in part by the US DoE multi-machine Joint Research Milestone in 2010, which seeks to understand thermal transport in the SOL through experiments on Alcator C-Mod, DIII-D and NSTX. Correspondingly, results from DIII-D [3,4] and C-mod [5,6] are being reported at this conference. In addition, the planned upgrade on NSTX (NSTX-U) [7] will increase plasma current, $I_p \leqslant 2$ MA; neutral beam heating power, $P_{NBI} \leqslant 10$ MW; and a pulse length of 5 s have motivated further work on understanding the scaling of λ_q^{mid} (where $\lambda_q^{mid} = \lambda_q^{div}/f_{exp}$ and f_{exp} is the magnetic flux expansion) with P_{NBI} and I_p, particularly for highly shaped plasmas. Previous estimates [8] indicated that a heat flux of 10 MW/m^2 would exceed the 1200 C administrative limit of the ATJ graphite tiles in about 3 s short of the desired pulse length of 5 s.

NSTX has previously measured the dependence of the outer perpendicular divertor peak heat flux, $q_{div,\ peak}$, on controlled engineering parameters [9,11]; a preliminary assessment of the divertor heat flux widths was also made in these experiments. Here we present systematic analysis of the divertor heat flux widths from both those experiments and new ones, for projection to the planned NSTX-U. The planned upgrade to NSTX will stress the thermal limits of NSTX's graphite PFCs with neutral beam input power, $P_{NBI} \leqslant 12$ MW; RF heating power, $P_{RF} \leqslant 6$ MW; toroidal magnetic field, $B_t \leqslant 1$ T; $I_p \leqslant 2$ MA; and pulse lengths up to 5 s [10]. Viable divertor designs may require some combination of heat flux mitigation techniques, including some combination of a detached or radiative divertor [12], high magnetic flux expansion [13], and/or a snowflake divertor [14,15].

2. Experimental apparatus

NSTX is a medium-sized spherical torus with a major radius $R = 0.85$ m, minor radius, $a \leqslant 0.65$ m ($R/a \geqslant 1.27$), $I_p \leqslant 1.4$ MA, $B_t \leqslant 0.55$ T, $P_{NBI} \leqslant 7.4$ MW, $P_{RF} \leqslant 6$ MW, and pulse lengths of $\leqslant 1.8$ s. The NSTX open divertor geometry enables a wide range of discharge shapes, both high and low triangularity (δ) discharge shapes, shown in Fig. 1, as well as a range of magnetic flux expansions, f_{exp}.

* Corresponding and presenting author. Address: PO Box 451 MS-34, Princeton, NJ 08543-0451, USA. Tel.: +1 609 243 2212; fax: +1 609 243 2874.
E-mail address: tkgray@pppl.gov (T.K. Gray).

0022-3115/$ - see front matter © 2011 Elsevier B.V. All rights reserved.
doi:10.1016/j.jnucmat.2011.01.029

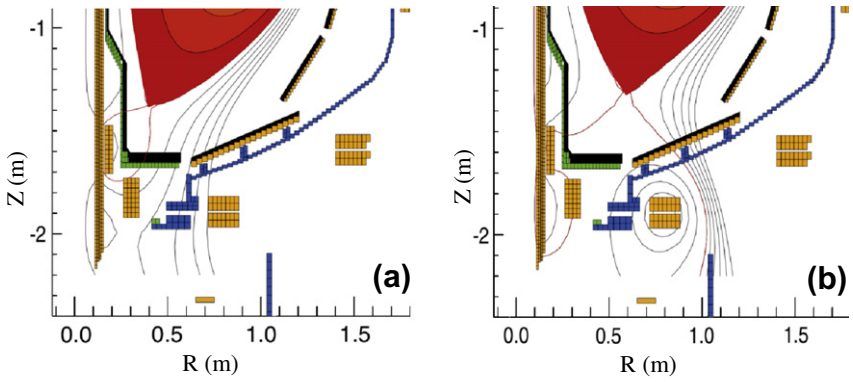

Fig. 1. Efit01 equilibrium reconstructions for two discharges with different plasma shapes. (a) High δ discharge (shot # 128,640, 0.4 s) with $\delta \sim 0.7$, $\kappa = 2.3$ and $f_{exp} = 16$. (b) Low δ discharge (shot # 132,341, 0.41 s) with $\delta \sim 0.44$, $\kappa = 2.1$ and $f_{exp} = 4$.

Surface IR emissivity measurements are captured by an Indigo Omega camera at a 30 Hz frame rate, with surface temperature derived from both an *ex situ* calibration with a blackbody calibration source and an *in situ* calibration during vacuum bake-outs [16]. Since 2006 NSTX has employed evaporative lithium wall conditioning on its ATJ graphite plasma facing surfaces during some or all of the run campaign [17]. The key results presented in Sections 3.1–3.3 are for discharges with boronized walls and *not* with lithium wall conditioning. This is because the application of thin lithium films alters the surface emissivity of graphite tiles, and the surface emissivity could be continuously modified due to the chemical reactivity of lithium and the erosion and redeposition of the lithium films during a discharge.

All of the data presented here are for lower single null (LSN), deuterium H-mode discharges, with line averaged electron densities, $\bar{n}_e = 4\text{–}7 \times 10^{19}$ m^{-3}; $B_t \cong 0.45$ T; and the magnetic balance, δ_r^{sep} between 0.005 and 0.015 m. δ_r^{sep} is defined as the radial distance between the upper divertor separatrix flux surface and the lower divertor separatrix flux surface as measured at the outer mid-plane. Given the 30 Hz frame rate of the IR camera system, measurements obtained are averaged over small edge localized modes (ELMs), which are ubiquitous through out the H-mode phase of the discharges. Time slices just after large transients, disruptions or large Type-I ELMs that result in a large, rapid decrease ($\geqslant$10%) in the plasma stored energy, W_{MHD}, have been removed from the scaling analysis.

Fig. 2 shows typical discharge parameters along with the measured change in divertor surface temperature, $\Delta T_{div,\ peak}$, and $q_{div,\ peak}$. Heat flux is calculated based on a 1-D, semi-infinite heat conduction approximation [18,20]. The peak divertor temperature rise (Fig. 2d) flattens as $\bar{n}_e$ rises continuously through out the discharge. This secular density rise in boronized NSTX discharges is believed to be due to a strong fueling source at the inboard divertor strike point, which is typically detached [19]. The peak divertor heat flux is reached at ~0.35 s and then decreases as the density rises. However, the power to the outer divertor remains constant, shown in Fig. 2g, after the peak heat flux is reached. This is due to a broadening of the divertor heat flux profile (Fig. 2f). Because of the secular $\bar{n}_e$ rise, the data presented are limited to 100–200 ms windows after the onset of H-mode and after W_{MHD} has reached steady state. Changes in $\bar{n}_e$ and δ_r^{sep} with in this time window do not appear to affect the width of the heat flux footprint. For example the analysis

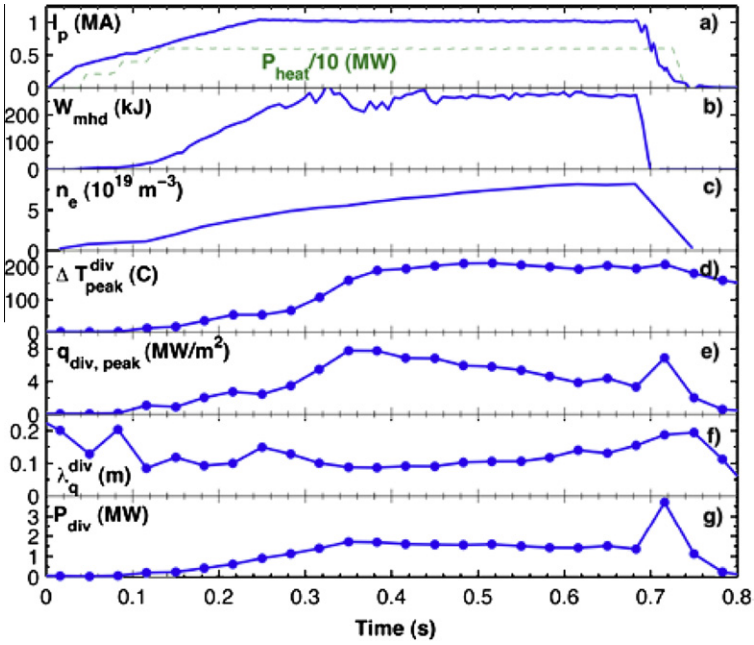

Fig. 2. Typical progression of discharge parameters for NSTX (shot # 128,640) in (a) I_p and P_{heat}, (b) plasma stored energy, W_{MHD}, (c) $\bar{n}_e$, (d) ΔT^{div}_{peak}, (e) $q_{div,\ peak}$, (f) λ^{div}_q and (g) power to the outer divertor, P_{div}.

window for the discharge shown in Fig. 2 is from 0.3 to 0.5 s. While this results in a conservative estimate of the heat flux width scaling with respect to the present discharges, future operation in NSTX and NSTX-upgrade should result in steady density profiles. We anticipate execution of experiments with density in the lower range shown in Fig. 2c in NSTX-U, and so the projections and divertor designs for NSTX-U should accommodate such experiments.

3. Results

As described earlier, the measurements obtained are averaged over edge localized modes (ELMs) [21], as routinely observed in NSTX discharges with boronized walls. In order to compare results from NSTX to those of other tokamaks, an integral definition of the characteristic scale length, λ_q^{div} of the heat flux is used. While this definition of λ_q^{div} differs from the one used in previous work [9,11], the integral definition facilitates comparison across devices, as was discussed in [22]:

$$\lambda_q^{div} \equiv \frac{P_{div}^{out}}{2\pi R_{div,\,peak}^{out} q_{div,peak}^{out}}, \quad (1)$$

where $q_{div,\,peak}^{out}$ is the peak in the divertor heat flux measured from IR thermography, $R_{div,\,peak}^{out}$ is the radial location the peak heat flux occurs, and P_{div}^{out} is the outer divertor power derived from the measured divertor heat flux defined as,

$$P_{div}^{out} = \int_{R_{min}}^{R_{max}} 2\pi R_{div}^{out} q_{div}^{out} dr, \quad (2)$$

where $R_{min} - R_{div,\,peak} = -0.05$ m and $R_{max} - R_{div,\,peak} = 0.20$ m. λ_q^{div} is then magnetically mapped to the mid-plane such that $\lambda_q^{mid} = \lambda_q^{div}/f_{exp}$, where f_{exp} is the average magnetic flux expansion measured at the outer strike point along the ~5 mm mid-plane flux surface, and defined as $f_{exp} = \left(R_{mid}B_\theta^{mid}\right)/\left(R_{div}B_\theta^{div}\right)$. B_θ^{mid} and B_θ^{div} are the mid-plane and divertor poloidal magnetic fields at radial locations R_{mid} and R_{div} respectively.

3.1. λ_q^{mid} scaling with magnetic flux expansion

The magnetic flux expansion was varied by changing the x-point height in NSTX. Highly shaped ($\delta \sim 0.8$, elongation, $\kappa \cong 2.2$–2.4), lower single null H-mode discharges were performed [13] with $I_p = 1.0$–1.2 MA and $P_{NBI} = 6$ MW. Fig. 3 shows that $q_{div,\,peak}$ is reduced from 8 MW/m^2 to 2 MW/m^2 by increasing f_{exp} from 10 and 40. This is because as f_{exp} is increased, λ_q^{div} broadens as shown in Fig. 3b, where λ_q^{div} increases monotonically from 10 to 37 cm as a function of f_{exp}. This is due to the large magnetic flux expansion is acting to increase the plasma wetted area on the divertor and therefore increase the area over which energy must be dissipated. Note the two outlying data points with high peak heat fluxes, $q_{div,\,peak} \geqslant 7$ MW/m^2, both at $f_{exp} \cong 27$, while the majority of the data at similar f_{exp} have $q_{div,\,peak} \leqslant 4$ MW/m^2. These data are included for completeness, as they cannot be directly attributed to any identifiable transient heat load on the divertor such as large Type-I ELMs. When λ_q^{div} is magnetically mapped to the mid-plane as in Fig. 3c, the variation in the λ_q^{mid} is 0.95 ± 0.2 cm. Therefore, while $q_{div,\,peak}$ scales inversely with f_{exp}, the λ_q^{mid} is largely independent of f_{exp}.

3.2. λ_q^{mid} scaling with P_{LOSS}

Fig. 4 shows that as P_{LOSS} is increased from 0.5 to 6 MW, the peak heat flux increases as expected. Here P_{LOSS} is defined as $P_{LOSS} = P_{NBI} + P_{oh} - dW/dt - P_{rad}^{core}$, where P_{oh} is the ohmic input power, dW/dt is the time rate of change of the plasma energy,

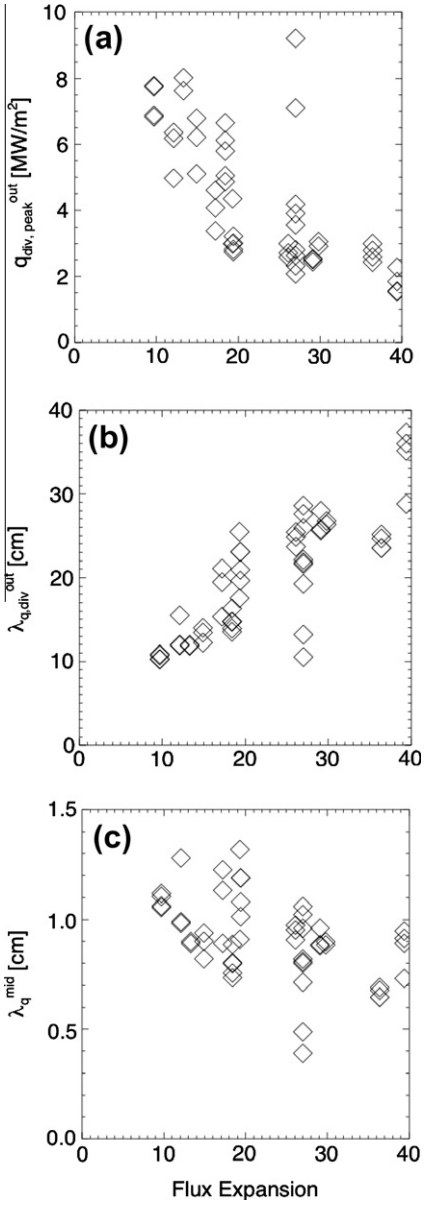

Fig. 3. Effect of magnetic flux expansion as measured at the outer strike point for high triangularity discharges. (a) Reduction in peak heat flux as f_{exp} is increased. (b) Broadening of the heat flux profile, λ_q^{div} as f_{exp} is increased. (c) λ_q^{div} magnetically mapped to the mid-plane, λ_q^{mid} modestly shrinks with f_{exp}.

and P_{rad}^{core} is the core radiated power. For low δ discharges ($\delta \sim 0.5$, $I_p = 0.8$ MA), there is a marked decrease in λ_q^{mid} as P_{LOSS} is increased beyond 4 MW, shifting from an average λ_q^{mid} of approximately 3 cm down to 1.5 cm. This is due to a transition from a radiative (or possibly even partially detached) divertor to an attached, high recycling divertor at $P_{LOSS} \geqslant 4$ MW. The radiated power drops as P_{LOSS} is increased and is consistent with previous 2-point modeling [11,23], where the transition to an attached divertor is denoted by a change in slope of $q_{div,\,peak}$ vs. P_{LOSS} as shown in Fig. 4a. We note, however, that a detailed analysis of the divertor regime (as previously done in NSTX [24]) to determine if detachment and volume recombination are occurring has not yet been performed. For the high δ discharges shown in Fig. 4b, where $\delta \sim 0.7$, $f_{exp} = 16$ and $I_p = 1.2$ MA, λ_q^{mid} is constant at ~0.7 cm. Note that the data for high δ discharges are chosen where $P_{LOSS} \geqslant 5$ MW. Therefore, λ_q^{mid} appears to vary weakly with P_{LOSS}, when the divertor is in an attached regime. We will show in the next section that

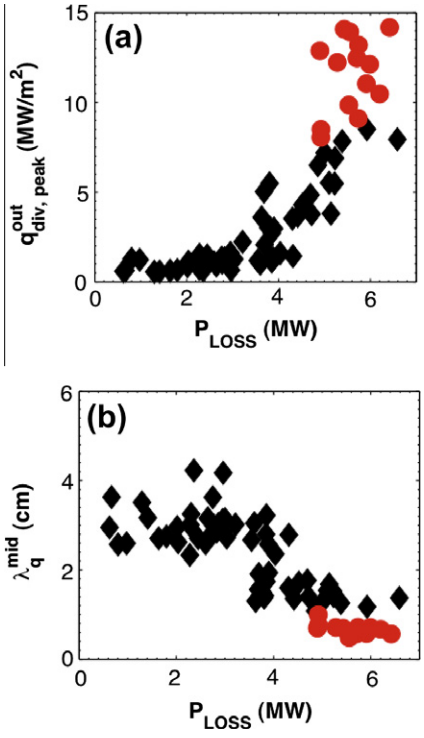

Fig. 4. Scan of power lost through the last closed flux surface, P_{LOSS} for low triangularity (♦) and high triangularity (●) discharges. (a) Outer divertor peak heat increasing as P_{LOSS} increases with the change in slope denoted by the vertical dashed line. (b) Reduction in λ_q^{mid} as P_{LOSS} is increased beyond 4 MW suggesting a change in divertor regimes from detached/radiative to attached.

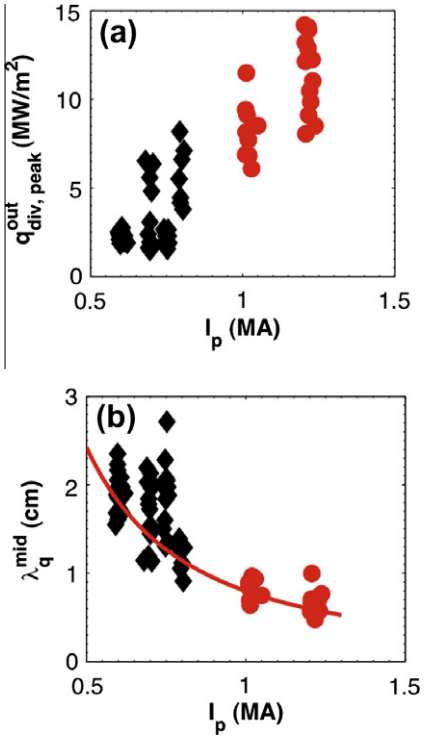

Fig. 5. Effect of increasing plasma current, I_p for low triangularity (♦) and high triangularity (●) discharges. (a) Outer divertor peak heat flux increases with increasing plasma current. (b) λ_q^{mid} contracts with increasing plasma current. (——) Power law fit to the λ_q^{mid} data.

this difference in λ_q^{mid} values between low and high δ are actually due to a strong I_p dependence in the data.

3.3. λ_q^{mid} scaling with plasma current

Since the results of the previous two sections showed λ_q^{mid} is largely independent of f_{exp} and P_{LOSS}, Fig. 5 shows that the heat flux and λ_q^{mid} depend on I_p. Here we include low δ discharges ($\delta \sim 0.5$) with $P_{NBI} = 4$ MW and $f_{exp} = 6$, as well as high δ discharges ($\delta \sim 0.7$) with $f_{exp} = 16$ and $P_{NBI} = 6$ MW. The minimal dependences of λ_q^{mid} on other parameters have probably resulted in some of the scatter in Fig. 5. Fig. 5b shows that λ_q^{mid} strongly contracts with increasing I_p such that $\lambda_q^{mid} = 0.91\ I_p^{-1.6\pm0.1}$. Here, only the lower 20% of the data set was considered to provide a conservative estimate of the I_p scaling for NSTX-U. Note that both DIII-D [25] and JET [26] have reported similar trends where λ_q^{mid} is inversely proportional to I_p; DIII-D in particular has reported $\lambda_q^{mid} \propto I_p^{-1.2}$ [3], close to the NSTX result.

Recent simulations of mid-plane SOL turbulence with the SOLT code [27] were performed for select NSTX discharges. It was concluded that mid-plane turbulence is the main contributor to the SOL heat flux width for the low power ELM-free H-mode discharges studied, while additional physics is required to explain the strong contraction of λ_q^{mid} with I_p observed experimentally in higher power discharges.

3.4. Effect of lithium wall conditioning

As previously stated, NSTX has been using lithium for wall conditioning for edge density control, higher confinement times [28], and the elimination of ELMs [29]. The change in surface emissivity due to the lithium coatings makes determining the divertor surface temperature, and therefore the magnitude of the heat flux, questionable with conventional IR thermography. However, the divertor heat flux profile could be less sensitive to emissivity changes. Fig. 6 shows the contraction of the heat flux profile with (shot # 129,038) and without (shot # 129,019) the application of evaporative lithium coatings for $I_p = 0.8$ MA and $P_{NBI} = 4$ MW for the no lithium discharge. However, in the case of the discharge with lithium, P_{NBI} was lowered to 2 MW to avoid β_N limits; therefore, λ_q^{div}, as defined in Eq. (2), is lower for shot # 129,038 consis-

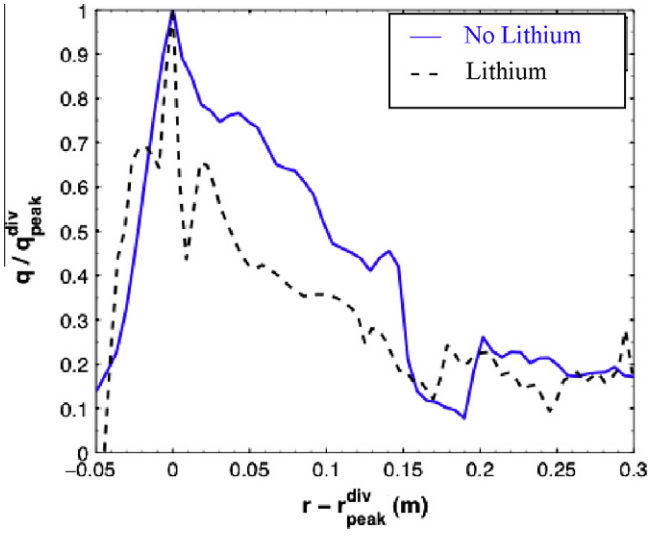

Fig. 6. Radial heat flux profile, in arbitrary units, showing the contraction in the heat flux profile at 0.662 s for two discharges: shot # 129,019, no-lithium wall conditioning (——) and shot # 129,038 with approximately 700 mg of lithium evaporation between the two shots (—).

tent with power accounting. For the profiles shown in Fig. 6, $\lambda_{q,exp}^{div}$, here defined as the e-folding length of the SOL side of the profile, contracts from 2.4 cm to 0.9 cm or a 62% decrease with the evaporation of approximately 700 mg of lithium between discharges. The post-lithium discharge profile itself is more Gaussian, lacking the long tail typically seen in the SOL region of divertor heat flux profiles from NSTX. An important difference between the two discharges is the elimination of small, Type V ELMs. Type V ELMs typically result in higher cross-field transport in the SOL and may explain the contraction of $\lambda_{q,exp}^{div}$. A two color-IR camera has been developed for NSTX to quantify the heat flux profile with lithium coatings [30]. The system has been designed to be less sensitive to emissivity changes that occur because of the lithium wall conditioning and will be used to confirm these preliminary results.

4. Summary and conclusions

It has been shown that for neutral beam heated, H-mode discharges in NSTX $\lambda_q^{div} \propto f_{exp}$, while $q_{div,peak} \propto 1/f_{exp}$. However, when λ_q^{div} is mapped to the mid-plane, it is relatively independent of f_{exp}. Additionally, λ_q^{mid} is independent of P_{LOSS} in well-attached, high recycling plasmas with high P_{LOSS}. In contrast, λ_q^{mid} is found to vary $\propto I_p^{-1.6}$, with $q_{div,\ peak}$ reaching 15 MW/m^2 when I_p = 1.2 MA and P_{NBI} = 6 MW. The I_p scaling covers a wide range of plasma shapes, flux expansions and heating powers. Preliminary data show $\lambda_{q,\ exp}^{div}$ is further reduced by as much as 60% with lithium wall conditioning, which results in ELM-free discharges. Future experiments are planned to further explore the effect of lithium wall conditioning using a 2-color IR diagnostic [30] that should be less susceptible to emissivity changes on the divertor tiles.

To project for NSTX-U [7], Eq. (1) can be re-written to estimate the peak heat flux on the divertor such that $q_{div,peak}^{out} = P_{div}^{out}/(2\pi R_{div,peak}^{out} f_{exp} \lambda_q^{mid})$, where $P_{div}^{out} \approx f_{div} P_{heat}$, $f_{div} = 0.5$ and $\lambda_q^{mid} \approx 0.9 I_p^{-1.6}$. Therefore, for I_p = 2 MA, P_{NBI} = 12 MW and $\delta \sim 0.7$, the peak heat flux to the divertor would reach 24 ± 4 MW/m^2 for f_{exp} = 30. It is evident that some technique of heat flux mitigation such as even higher flux expansion, double null operation or radiative/detached divertor operation will be required for NSTX-U as 24 MW/m^2 would exceed the established material limits of ATJ graphite for the 5 s design pulse lengths.

Acknowledgements

The authors are grateful to the NSTX research team for diagnostic and technical support. T.K. Gray is supported under an appointment to the US DOE. Fusion Energy Postdoctoral Research Program administered by the Oak Ridge Institute for Science and Education under Contract Number DE-AC05-06OR23100 between the US DOE and Oak Ridge Associated Universities. This research is sponsored by US DOE Contracts DE-AC05-00OR22725, DE-AC52-07NA27344, and DE-AC02-09CH11466.

References

[1] G.F. Counsell et al., J. Nucl. Mater. 266–269 (1999) 91–98.
[2] M. Ono et al., Nucl. Fusion 40 (2000) 557–561.
[3] C.J. Lasnier et al., these proceedings.
[4] M. Makowski et al., these proceedings.
[5] B. LaBombard et al., these proceedings.
[6] D. Brunner et al., these proceedings.
[7] J.E. Menard, et al., in: Proceedings of the 37th EPS Conference on Plasma Phys., 2010.
[8] R. Maingi et al., Plasma Phys. Control. Fusion. 45 (2003) 657.
[9] R. Maingi et al., J. Nucl. Mater. 313–316 (2003) 1005–1009.
[10] C. Neumeyer et al., Fusion Eng. Des. 54 (2001) 275–319.
[11] R. Maingi et al., J. Nucl. Mater. 363–365 (2007) 196–200.
[12] V.A. Soukhanovskii et al., Phys. Plasmas 16 (2009) 022501.
[13] V.A. Soukhanovskii et al., Nucl. Fusion 49 (2009) 095025.
[14] D.D. Ryutov, Phys. Plasmas 14 (2007) 064502.
[15] V.A. Soukhanovskii et al., these proceedings.
[16] D.M. Mastrovito et al., Rev. Sci. Instrum. 74 (12) (2003) 5090–5092.
[17] H.W. Kugel et al., Phys. Plasmas. 15 (2008) 056118.
[18] D.N. Hill et al., Rev. Sci. Instrum. 61 (1990) 3548.
[19] V.A. Soukhanouvskii et al., J. Nucl. Mater. 390–391 (2009) 516–519.
[20] C.J. Lasnier et al., Nucl. Fusion. 38 (1998) 1225.
[21] R. Maingi et al., Nucl. Fusion. 45 (2005) 264.
[22] A. Loarte et al., J. Nucl. Mater. 266–269 (1999) 587–592.
[23] K. Borass et al., Nucl. Fusion 31 (1991) 1035.
[24] V.A. Soukhanovskii et al., J. Nucl. Mater. 337–339 (2005) 475–479.
[25] C.J. Lasnier, Bull. Am. Phys. Soc. (2009).
[26] W. Fundamenski, Private Communication, 2009.
[27] J.R. Myra et al., these proceedings.
[28] M.G. Bell et al., Plasma Phys. Control. Fusion 51 (2009) 124054.
[29] R. Maingi et al., Phys. Rev. Lett. 103 (7) (2009) 075001.
[30] A.G. McLean et al., Rev. Sci. Instrum., submitted for publication.